Energy Equip. Sys./ Vol. 7/No. 4/Dec. 2019/ 377-387

ENERGY EQUIPSYS

Energy Equipment and Systems

http://energyequipsys.ut.ac.ir
www.energyequipsys.com

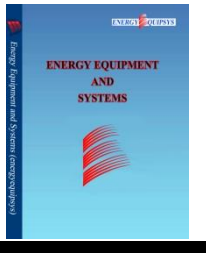

Parametric study of a novel oscillatory wind turbine

Authors

Radmarz Hosseini [a*]
Reza Roohi [a]
Goodarz Ahmadi [b]

[a] Department of Mechanical Engineering, College of Engineering, Fasa University, 74617-81189 Fasa, Iran

[b] Department of Mechanical & Aeronautical Engineering, Clarkson University, Potsdam, NY 13699-5725, USA

ABSTRACT

Clean energy harvesting and usage has gained considerable attention in the last few decades. While the horizontal axis wind turbines have been used extensively, they have certain defects and functional limitations. In the present paper, a novel oscillatory wind turbine is proposed. The conceptual design of the new turbine together with its configuration is explained. Dynamical equations of the turbine are derived and numerical analysis of these equations is performed using a developed computer code. The simulated behavior of the oscillatory turbine agrees well with the general behavior of the wind turbines, and the values for the power coefficient are acceptable for a micro-sized wind turbine.

Article history:

Received : 4 June 2019
Accepted : 3 November 2019

Keywords: Oscillatory Wind Turbine, Dynamical Governing Equations, Clean Energy Harvesting, Parametric Study.

1. Introduction

Clean energy harvesting has gained considerable attention in the last few decades. The fossil energy resources are gradually diminishing, and there are several environmental hazards encountered in the usage of fossil fuels. These facts have persuaded the engineers to concentrate on the clean and renewable sources of energy as the major part of the so-called 'sustainable engineering.' One of the widely used alternative energy sources is wind energy. Wind energy harvesting is developing rapidly around the world, especially in Europe and North America [1-7].

Among the conventional wind turbine types, which are commercially developed and used in harvesting wind energy, are the horizontal axis wind turbines. This is even though other types of wind turbines such as vertical axis wind turbines are also used and have become commercial, albeit not as common as the horizontal axis designs.

Despite the common use, the horizontal wind turbines have certain defects and functional limitations. One of the most life-limiting defects of this type of turbines is the wearing that happens in the rotating parts (bearings and gears) due to the stochastic load of the wind [8-10]. Although, there has been a vast effort to overcome or to reduce these defects by modifying the design of horizontal wind turbines, or by prognosis these defects [8, 10], these limiting defects have become the source of motivation for

[*] Corresponding author: Radmarz Hosseini
Department of Mechanical Engineering, College of Engineering, Fasa University, 74617-81189 Fasa, Iran
Email: Hosseini.r@fasau.ac.ir

engineers to search for and examine alternative designs [9]. One of the alternative designs can be 'non-rotary' wind turbine. In this design, the turbine can oscillate to harvest wind energy, and omits the problems and drawbacks caused by the rotating method.

In the present paper, a novel oscillatory wind turbine is proposed. First, the conceptual design of the new turbine together with its configuration, is explained. Then, the turbine equations of motion are presented. A set of turbine geometric and kinetic parameters is selected as benchmark parameters and the numerical simulation of the dynamical system using a developed computer code is performed. The results for the generated power, as well as the power coefficient of the benchmarked turbine, show the possibility of utilizing this novel design as a wind turbine in harvesting wind energy.

1.1. Physical Configuration of the Turbine and its Operation

The proposed schematic of the oscillatory turbine is shown in Fig. 1. The turbine is composed of several parts. (1) Sail: A light rectangular plate which is held against the wind and pushed ahead using the drag generated by the wind. (2) Mast: A long beam that carries the sail and is hinged to the ground (at axis O_1 in Fig. 1). A rotational spring attached to the mast causes the mast to oscillate around axis O_1. (3) Flywheel: a heavy wheel mounted on the axis O_1 and rotated around it. The mast and the flywheel are attached by a ratchet mechanism.

Assuming the wind blows horizontally and from left to right, once the wind pushes the sail ahead and, consequently, the when mast oscillates to the right (according to Fig. 1), the flywheel rotates clockwise. This motion is the empowering stroke of turbine operation, *i.e.,* the stroke in which the power of wind is transferred to the flywheel. As the sail lies horizontal, the drag force drops down, and the mast rocks back to the left due to the rotational spring. In this stroke, the flywheel retains its clockwise rotation and does not return with the mast. This one- way rectified motion is performed by the ratchet.

In the preliminary study of the present turbine, the gearbox and the generator are omitted from the configuration of the turbine, in order to simplify the analysis. For power and efficiency investigations, a constant dynamometric torque is assumed to apply on the flywheel.

The angle of the sail relative to the wind must be controlled and changed as a proper function of time in order to harvest the wind energy. To make the turbine oscillate, the angle of the sail must change periodically, so the drag force changes periodically and causes the mast to oscillate. The angle of the sail is controlled by a mechanism or a servo motor. The control system must be placed on the mast. The effect of servomotor or mechanism is represented by torque M_2 in Fig. 1.

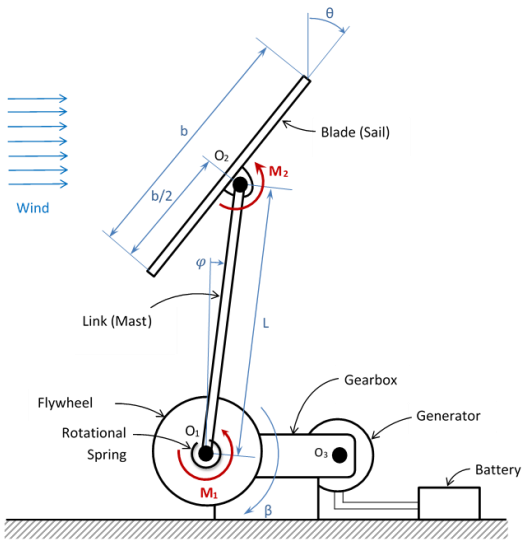

(a)

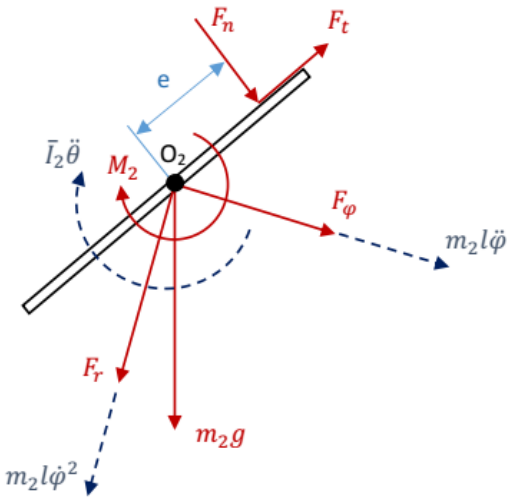

(b)

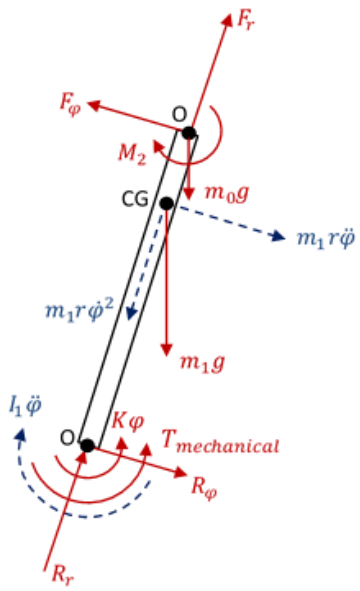

(c)

Fig.1: (a) Configuration of the proposed turbine (b) free body diagram of the sail (c) free body diagram of the mast

The angle of the sail can be controlled actively or passively. Here, it is assumed that the control method is passive and feedforward, *i.e.,* we predefine a periodic function for the angle of sail. For the preliminary model, a sinusoidal function is utilized. The sail angle must oscillate between $0^o$and 90^o sinusoidal as given by

$$\theta(t) = \frac{\pi}{4}\left[\sin\left(\frac{2\pi t}{T} + \frac{\pi}{2}\right) + 1\right]. \quad (1)$$

Hence, the angular speed and angular acceleration of the sail to be predefined functions of time either.

2. Mathematical Model of the Wind Turbine

2.1. The Governing Equations of Motion

In deriving the equation of motion of the sail, the following simplifications are assumed: (1) The axis of sail passes from the center of gravity of the sail; (2) The thickness of the sail is negligible.

According to the configuration of the mechanism shown in figure 1, θ is the angle of the sail with the vertical direction, φ is the angle of the mast with the vertical direction, and β is the angle of rotation of the flywheel. The most appropriate dynamical variables of the system are θ, φ, and β

Newton's second law of motion for the positive direction of φ, and the Euler equation around the CG of the sail are given as

$$m_2 l\ddot{\varphi} = F_\varphi + F_n cos\alpha + F_t sin\alpha + m_2 g sin\varphi \quad (2)$$

and

$$\bar{I}_2\ddot{\theta} = eF_n + M_2, \quad (3)$$

where $\alpha = \theta - \varphi$, F_φ is the force exerted from the mast on the sail in φ direction, F_n is the normal component of the aerodynamic force exerted on the sail, F_t is its tangential component, e is the aerodynamic force center, M_2 is the control moment acting on the sail to control its angle, m_2 is the mass of the sail, and $\bar{I}_2$ is its mass moment of inertia around its CG (point O_2).

Assuming the distance from the CG of the mast to axis O_1 is r, the Euler's equation of rotation for the mast around point O_1 is given by

$$(\bar{I}_1 + m_1 r^2)\ddot{\varphi} = -T_{mechanical} - K\varphi + m_1 g r sin\varphi - F_\varphi l - M_2, \quad (4)$$

where m_1 is the mass of the mast, $\bar{I}_1$ is its rotational inertia around its CG, m_0 is the mass of servomotor package and $T_{mechanical}$ is the coupling torque between the mast and the flywheel. Substituting for F_φ from the Eq.(3) gives

$$(\bar{I}_1 + m_1 r^2)\ddot{\varphi} = -T_{mechanical} - K\varphi - M_2 + g(m_1 r + m_2 l)sin\varphi - m_2 l^2 \ddot{\varphi} + l(F_n cos\alpha + F_t sin\alpha), \quad (5)$$

where, as before, $\alpha = \theta - \varphi$.
The equations of motion for the flywheel are given as

$$(I_1 + m_0 l^2 + m_2 l^2)\ddot{\varphi} + K\varphi - (m_1 r + m_2 l + m_0 l)gsin\varphi = l(F_n cos\alpha + F_t sin\alpha) - M_2 - T_{mechanical} \quad (6)$$

and

$$J\ddot{\beta} + d_{viscous}\dot{\beta} = T_{mechanical} - T_{resisitive}\ , \quad (7)$$

where J is the rotational inertia of the flywheel, $d_{viscous}$ is the total equivalent viscous damping coefficient of the turbine, and $T_{resisitive}$ is the resistive torque exerted on the flywheel by the dynamometer.

During the forward stroke, the mast carries the flywheel, which is possible only if the rotational speed of the mast is at the point of exceeding the rotational speed of the flywheel. At that moment, the mast and the flywheel collide and become coupled. Assuming the collision to be fully plastic, they will have equal angular speeds and angular accelerations after the collision. If the angular speed of the flywheel becomes higher than the angular speed of the mast algebraically, the mast cannot push the flywheel anymore and the separation and decoupling of the dynamical systems occurred. At the decoupling mode $T_{mechanical}$ vanishes.

It is possible to represent the coupling/decoupling dynamical phases just by comparing the angular speed of the mast and flywheel, considering their algebraic signs. Consequently, we can summarize the dynamics of the wind turbine in the following conditional equations:

If $\dot{\varphi} < \dot{\beta}$, the turbine is at its *decoupling phase*, whereby

$$(\bar{I}_1 + m_1 r^2 + m_2 l^2 + m_0 l^2)\ddot{\varphi} + K\varphi - (m_1 r + m_2 l + m_0 l)gsin\varphi = l(F_n cos\alpha + F_t sin\alpha) - M_2, \quad (8)$$

and

$$J\ddot{\beta} + d_{viscous}\dot{\beta} = -T_{resistive} \quad (9)$$

There is no power transmission from wind to the generator in this phase. The flywheel rotates solely due to its inertia.
Otherwise, the turbine is at its *coupling phase*, whereby

$$(\bar{I}_1 + m_1 r^2 + m_2 l^2 + m_0 l^2 + J)\ddot{\varphi} + d_{viscous}\dot{\varphi} + K\varphi - (m_1 r + m_2 l + m_0 l)gsin\varphi = l(F_n cos\alpha + F_t sin\alpha) - M_2 - T_{resistive}. \quad (10)$$

The coupling phase is the empowering phase of the turbine motion, where the power is transmitted from wind to the dynamometer.

2.2. The Aerodynamics of the Sail

The aerodynamic forces as the main turbine driving factor should be accurately modeled and implemented in the numerical simulation. For this purpose, the wind tunnel experimental investigation of Ortiz et al. (2015) [11] is utilized in the present study. They measured the steady and instantaneous components of aerodynamic forces and moments of a flat plate in a wind tunnel. They consider a wide range of plate aspect ratios (up to 9) and angle of attacks, as well as the clearance distance between the plate and the ground.

The drag and lift coefficients of sail plate are extracted from the experimental results of [11] and fitted to form appropriate expressions given as

$$C_d = (b_0 + b_1\alpha + b_2\alpha^2 + b_3\alpha^3)(a_0 + a_1 AR + a_2 AR^2 + a_3 AR^3), \quad (11)$$

$$C_l = (b_0 + b_1\alpha + b_2\alpha^2 + b_3\alpha^3)(a_0 + a_1 AR + a_2 AR^2 + a_3 AR^3) \quad (12)$$

In the above equations α, AR, C_d and C_l, are the plate angle of attack, aspect ratio, drag and lift coefficients, respectively. The constant parameters of Eqs. 11 and 12 are calculated and illustrated in Table 1.

Table 1. Constant parameters for C_d and C_l evaluation

	b_0	b_1	b_2	b_3
C_d	-0.8698	-0.1443	-0.00201	2.04E-5
C_l	-0.1896	0.1758	-0.00329	1.53E-5
	a_0	a_1	a_2	a_3
C_d	-0.0765	0.0034	-0.00081	4.78E-5
C_l	0.2930	0.0286	-0.01064	0.00079

It should be pointed out that the estimation of lift and drag forces exerted on the sail plate during its transient motion is based on the experimental data for a sequence of steady configurations. Therefore, utilization of Eqs. (11) and (12) assumes that the sequence of steady measurements is equivalent to the transient drag and lift acting on the sail. While this is a reasonable assumption, for slow to moderate range of sail velocity, the influence of transient flow pattern around the plate, as well as the possible formation of detaching vortices behind the plate, may cause some deviations from the steady experimental data at higher speeds.

The angle of attack of the sail, $\alpha = \theta - \varphi$, changes periodically as a function of time, due to the oscillations of θ, according to Eq.(1). This causes C_d and C_l to change periodically as functions of time according to Eqs. (11) and (12).

2.3. The Power and C_P Calculations

The supplied power to the turbine from the wind is considered to be the total wind power exerted perpendicularly to the total area of the sail. That is,

$$P_{wind} = \frac{1}{2}\rho_{air} A U^3, \tag{13}$$

where U is the wind speed, ρ_{air} is the air density, and A is the sail area. Another source of power is the power consumed by the servomotor in order to rotate the sail. The servomotor power is calculated as

$$P_{servomotor} = M_2(\dot{\theta} - \dot{\varphi}), \tag{14}$$

where M_2 is the servomotor torque which is represented by Eq.(3), and $\dot{\theta} - \dot{\varphi}$ is the relative velocity between the sail and the mast. Positive values of the servomotor power are contributed to the input power, as negative values imply the work done by the turbine on the servomotor. Consequently,

$$P_{servomotor}^{input} = M_2(\dot{\theta} - \dot{\varphi}) \ if \ M_2(\dot{\theta} - \dot{\varphi}) > 0 \tag{15}$$

The generated power by the turbine is measured by the dynamometer resistive torque applied on the flywheel multiplied by the flywheel rotational speed. Hence,

$$P_{output} = T_{resisitive}\dot{\beta} \tag{16}$$

The generated power never becomes negative, as the mast can only rotate the flywheel in the positive direction, *i.e.,* clockwise, due to the convention in Fig. 1. The C_P, or efficiency, defined as the ratio of output power to the input power, is calculated as

$$C_P = \frac{T_{resisitive}\dot{\beta}}{\frac{1}{2}\rho_{air} A U^3 + [M_2(\dot{\theta} - \dot{\varphi})]_{positive}}. \tag{17}$$

2.4. The Generated Computer Code

A MATLAB code is developed to solve the system of nonlinear differential equations of the new turbine. The code solves the system of equations by utilizing a conventional Runge–Kutta order-4 algorithm [12]. Due to the dual-phase behavior of the turbine, *i.e.,* the coupled and decoupled phases of motion, the code includes an 'if condition'. At each time step, the code assumes the decoupled dynamics as default and solves the decoupled equations of motion. If the condition '$\dot{\varphi} < \dot{\beta}$' is satisfied for the end of the step, the decoupled assumption is correct; else, the step must be resolved for the coupled dynamics. It is noted that because the coupling phase may be satisfied at the first time step, it is difficult, if not impossible, to use the 'even function' of the MATLAB ODE.

Moreover, if $\dot{\varphi} < \dot{\beta}$ holds at the beginning of the time step and $\dot{\varphi} \geq \dot{\beta}$ holds for the end of the time step, then collision of the mast and the flywheel happens during the step. The reverse condition implies that the separation happens in the step.

3. Results and Discussion

3.1. Validity Investigation of the Code

Some pre-identified conditions with known results were run, and the results were examined to verify the reliability of the code. The static equilibrium happens if the torque generated by the aerodynamic force cannot overcome the resistive dynamometer torque. The static condition is fed to and tested by the code. The result agreed with the expected behavior.

Some further cases such as 'zero wind speed' along with 'nonzero initial angle of mast,' and 'zero weight condition', were also checked. The results agreed well with the expected behaviors.

3.2. Choice of a Benchmark Set of Parameters for the Turbine

To study the behavior of the turbine and to identify if the efficiency of the turbine is acceptable, a benchmark set of parameters is selected. These parameters are geometric and kinetic, as listed in Table 2. Because this parametric study is a pre-design study for building a prototype at Fasa University, the selected size for the benchmark turbine is in the range of 'micro-size' wind turbines, as these wind turbine types are suitable for low wind speeds. According to the Fasa meteorological wind data, the most abundant wind speed in Fasa is in the 'calm' or stagnant range, which has 44 to 68 percent of abundancy in different months. The most abundant wind speed after the calm regime is in the range of 2.1 to 3.6 m/s, which has 22 to 28 percent of abundancy in different months [13].

Table 2: Benchmark Parameters for the turbine

Quantity	Value	Units
Sail Height	1	m
Sail Width	1	m
Sail Total Area	2	m^2
Sail Aspect Ratio	1	-
Sail Area Density	0.1	Kg/m^2
Sail Oscillation Period	7	sec
Mast Length	2	m
Mast Length Density	0.2	Kg/m
Flywheel Inertia	10	$Kg.m^2$
Rotational Spring Constant	10	N.m/rad

In the preliminary benchmark turbine, the weight of the sail rotation mechanism, i.e., servomotor package, together with the effective viscous friction of turbine mechanical chain, are neglected.

3.3. Study the Time-Response of the Benchmarked Turbine

The results of the numerical simulation of the time response of the benchmark turbine are illustrated in Figs. 2-11. According to Fig. 2, the sail rotates harmonically, causes the mast to oscillate due to the wind force. The mast drifts to the right and oscillates around the angle $\varphi_0 \simeq +0 \cdot 175$ rad relative to the vertical direction. The angular bias from the vertical direction is because the wind blows from left to right.
The angular velocities of sail, mast, and flywheel are shown in Fig. 3. In the empowering phase, when the wind pushes the sail, the mast and flywheel are coupled and move together (the coupled phase is recognizable in Fig. 3, and is illustrated in detail in Fig. 7). When the aerodynamic force generated by wind on the sail becomes weak, the mast slows down and turns back, due to the act of rotational spring. This movement causes the mast and the flywheel to separate.

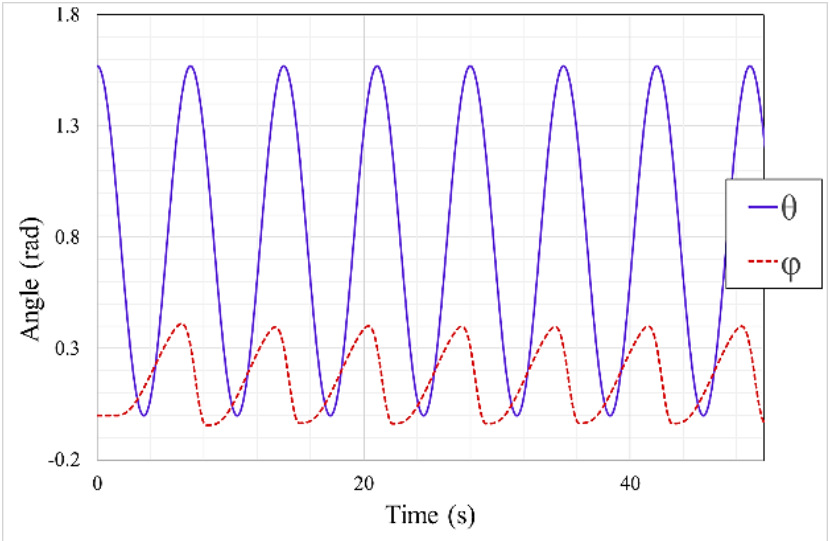

Fig.2. Time variation of angles of sail (θ) and mast (φ) for the benchmark turbine.

In the decoupled phase, the flywheel continues to rotate clockwise; however the mast oscillates counterclockwise. In time, the aerodynamic force on the sail increases again, the speed of the mast reaches the speed of the flywheel and they become coupled again. The coupling and decoupling events are recognizable more obviously and are discussed in detail in Fig. 7.

Figure 4 illustrates the angular accelerations of the sail, mast and flywheel. The piecewise behavior of flywheel acceleration is due to the sudden change and different behavior of the flywheel acceleration in coupling and decoupling phases of turbine motion.

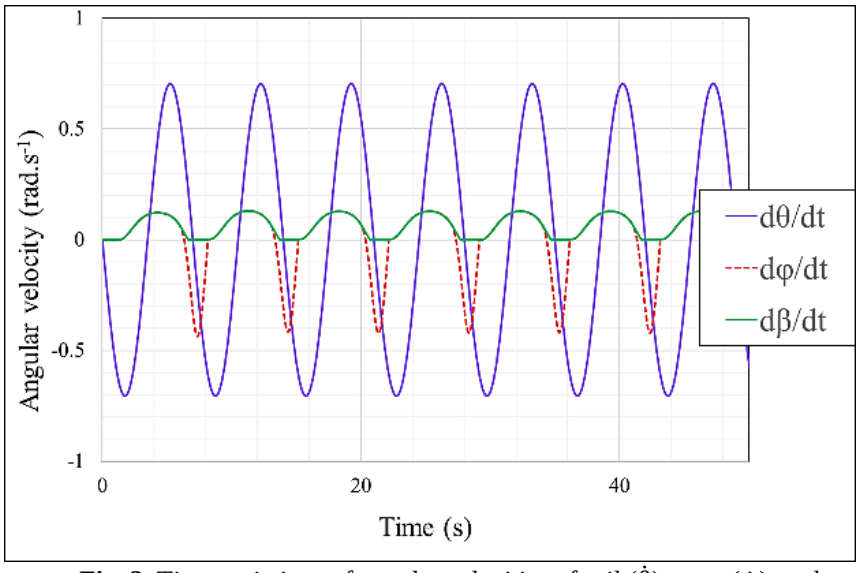

Fig. 3. Time variations of angular velocities of sail ($\dot{\theta}$), mast ($\dot{\varphi}$), and flywheel ($\dot{\beta}$) for the benchmark turbine.

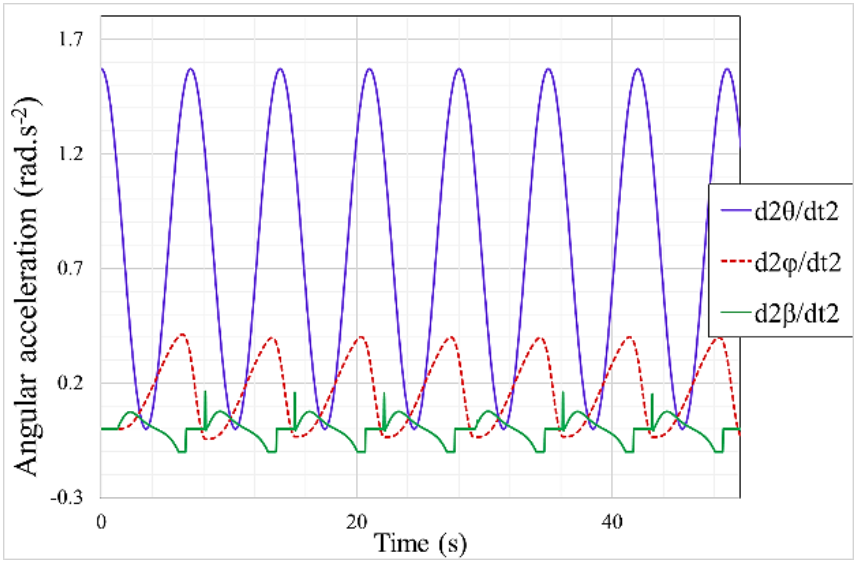

Fig.4. Time variations of angular accelerations of sail ($\ddot{\theta}$) mast ($\ddot{\varphi}$), and flywheel ($\ddot{\beta}$) for the benchmark turbine

In Fig. 5, the tangential and normal components of the aerodynamic force exerted by the wind on the sail are shown. The normal component is one order of magnitude higher than the tangential component in magnitude and has the primary role in empowering the turbine.

The coupling torque between mast and flywheel, together with the power generated by the turbine, is shown in Fig. 6. In the decoupled phase, the coupling torque and the generating power vanish. However, the power generation continues in this phase for a small duration, as the flywheel continues to rotate after it separates from the mast, due to its inertia. The flywheel decelerates and stops eventually as a result of the resistive torque. As the flywheel stops, there is no power generation, since the angular velocity of the flywheel becomes zero.

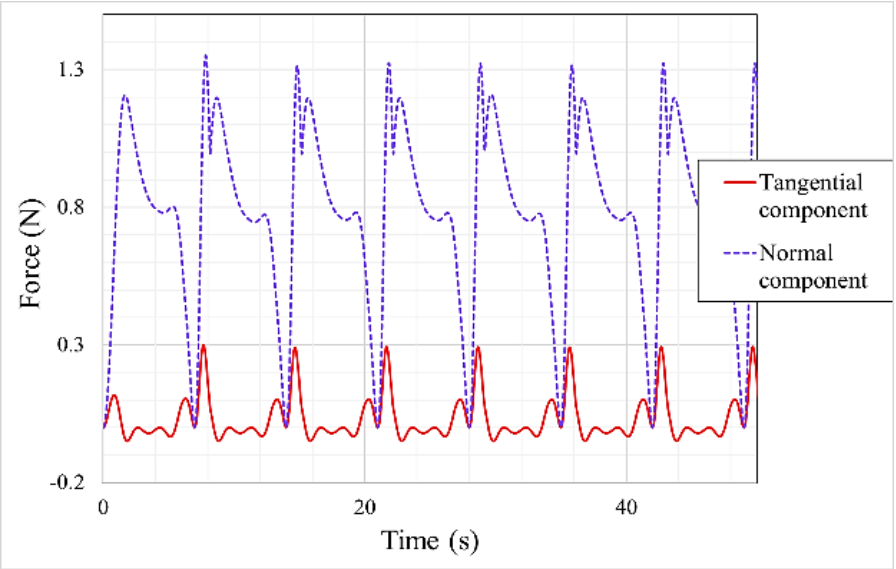

Fig.5. Time variations of the normal and tangential components of the aerodynamic force exerted on the sail by the wind for the benchmark turbine.

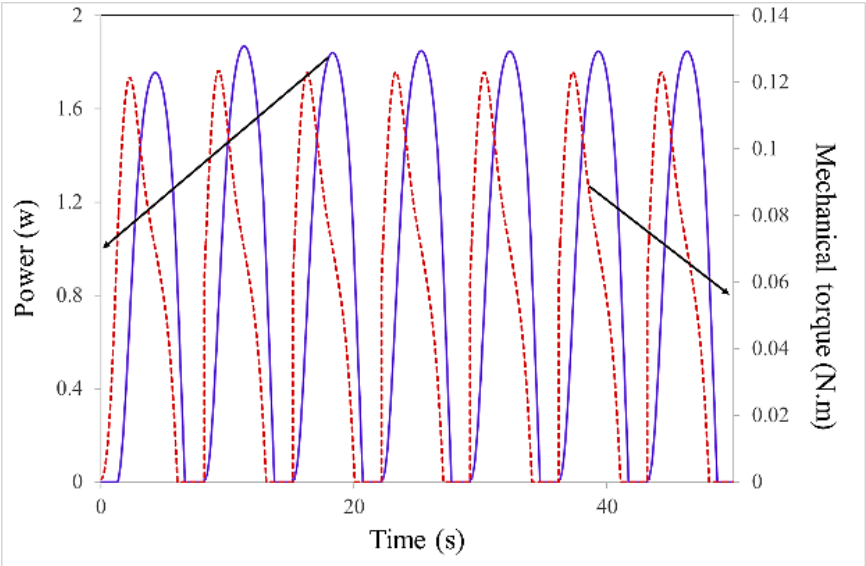

Fig. 6. Time variations of the mechanical torque (the coupling torque between mast and flywheel) and the power generated for the benchmark turbine

Figure 7 shows a close up of the small duration of turbine motion. Two consecutive separation and collision moments are shown. At the collision moment, an impulse in the acceleration of flywheel is seen. The abrupt change is due to the numerical error caused by the assumption in the MATLAB code that the angular velocities of flywheel and mast to be equal at the beginning of the time step in which collision happens. As it is evident, the acceleration decreases rapidly to its value before the impulse. Although this numerical error does not significantly affect the power and efficiency study of the turbine, this can be corrected by adding an iterative process to find the collision moment by interpolation, in the MATLAB code.

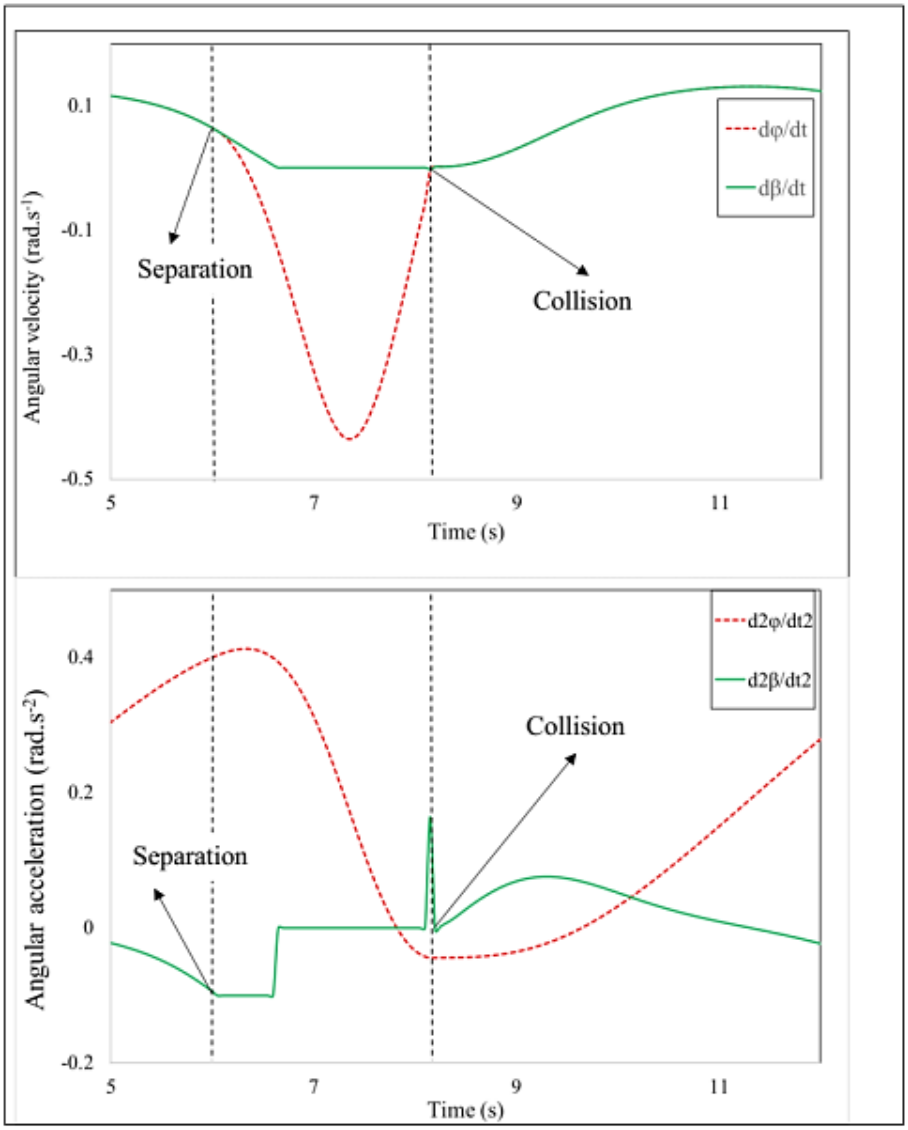

Fig.7. Close up of a small-time duration of the oscillations for the benchmark turbine

3.4. Study the Effect of Resistive Torque on the Behavior of the Benchmark Turbine

Figure 8 illustrates the power coefficient of the benchmark turbine for four different values of the resistive torque applied to the flywheel at different wind speeds. The selected range of the wind speed is the most recorded range at the Fasa meteorological node. As it is evident, for each selected value of the resistive torque, C_P is maximum in a certain wind speed, which means that the mentioned amount of resistive torque is the most appropriate for the benchmark turbine to work in that certain wind speed. By increasing the amount of resistive torque, the wind speed at which CP is maximum increases.

Figure 9 shows the power generated by the benchmark turbine for the four different values of the resistive torque. It is seen that at low wind speeds, the output power vanishes. At low wind speeds, the aerodynamic torque generated by the wind is not enough to overcome the resistive torque. Therefore, the turbine stands stationary and cannot oscillate, and consequently, there is no power generation.

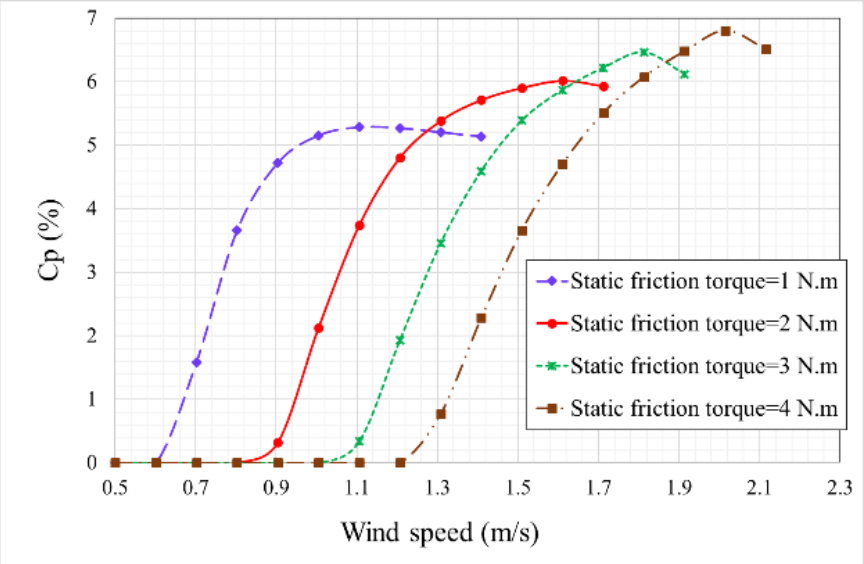

Fig.8. The power coefficient (C_P) of the benchmark turbine vs. wind speed at four different resistive torques.

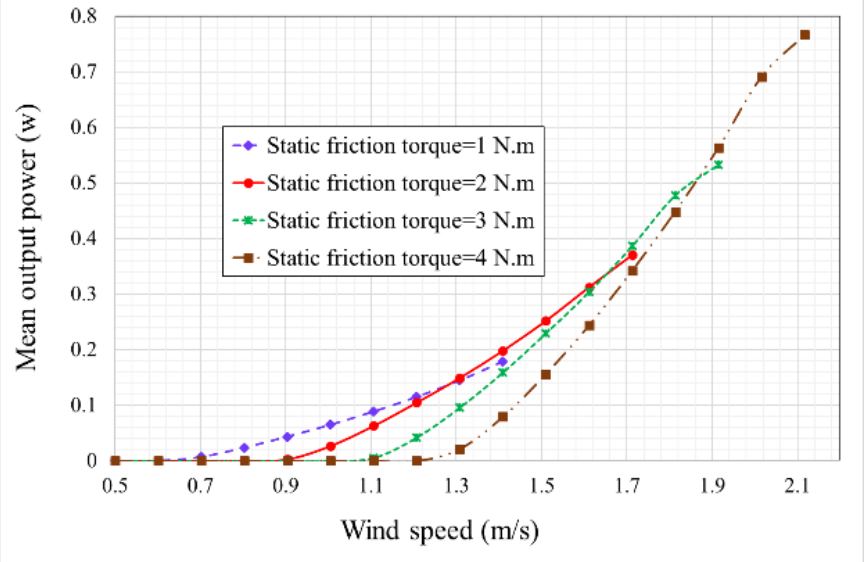

Fig.9. The power generated by the benchmark turbine vs. wind speed at four different resistive torques

4. Conclusion

The present research aimed to study the possibility of utilizing a novel design of oscillatory wind turbines to harvest wind energy. For this purpose, dynamical equations of the new turbine were derived and numerical analyzes using a developed computer code. The generated code was validated and then used to simulate the performance of a micro-sized benchmark wind turbine. The output power and the power coefficient of the benchmark turbine were examined for different resistive torques.

The behavior of the designed turbine agrees well with the expected behavior of these wind turbines, and the estimated values of the power coefficient are in the acceptable range for a micro-sized wind turbine.

As the continuation of this study, we plan to fabricate an experimental prototype for the benchmarked turbine and perform field testing. The presented simulations results can then be verified with the experimental data.

By the development of variant alternative wind turbines, it is hoped to surmount the drawbacks and defects of the conventional rotary wind turbines and to attain higher performance for specific ranges of wind speeds.

Acknowledgement

This work was supported by the Iran National Science Foundation (INSF) [Grant number 97022858].

References

[1] Hau, E., Wind Turbines: Fundamentals, Technologies, Applications, Economics. (2006) 2nd Ed, Springer – Verlag Berlin Heidelberg.

[2] EWEA (October 2009). "Wind Energy – the Facts, a Guide to the Technology, Economy, and Future of Wind Power," European Wind Energy Association. October 2009.

[3] EWEA (February 2013). “Wind will be cheapest electricity-generating technology by 2020”, European Wind Energy Association. 04 Feb. 2013.

[4] EWEA (February 2014). "Wind in power: 2013 European statistics", European Wind Energy Association. Retrieved 2014-11-05.

[5] Fraunhofer Institute (January 2015). "Electricity production from solar and wind in Germany in 2014 (German version)". Fraunhofer ISE website. Fraunhofer Institute, Germany. 5 January 2015. pp. 2, 3. Retrieved 5 January 2015.

[6] EWEA (February 2017) "Wind in power: 2016 European statistics", European Wind Energy Association. February 2017.

[7] AWEA (February 2017). "AWEA 2016 Fourth Quarter Market Report". American Wind Energy Association. Retrieved 9 February 2017.

[8] Musial, W., Butterfield, S., and McNiff, B., Improving Wind Turbine Gearbox Reliability, an NREL Publication, NREL/CP-500-41548, May 2007.

[9] DOE (2010) “Advanced Wind Turbine Drivetrain Concepts: Workshop Report,” a DOE Issue, 2010.

[10] NREL (2015). “NWTC Collaborative Increases Gearbox Reliability and Helps Reduce Cost of Wind Energy,” a National Renewable Energy Laboratory fact sheet, 2015.

[11] Xavier Ortiz, David Rival, and David Wood, Forces and Moments on Flat Plates of Small Aspect ratio with Application to PV Wind Loads and Small Wind Turbine Blades, Energies 2015, 8, 2438-2453.

[12] Steven C. Chapra, Raymond P. Canale, Numerical Methods for Engineers, 6th ed. Published by McGraw-Hill, New York, 2010.

[13] Iran Meteorological Organization (2015). “Wind Atlas of Fasa Meteorological Node.” (in Farsi)